View metadata, citation and similar papers at core.ac.uk

brought to you by CORE

provided by IntechOpen

We are IntechOpen, the world's leading publisher of Open Access books
Built by scientists, for scientists

5,000
Open access books available

125,000
International authors and editors

140M
Downloads

154
Countries delivered to

Our authors are among the
TOP 1%
most cited scientists

12.2%
Contributors from top 500 universities

CLARIVATE ANALYTICS
BOOK CITATION INDEX
INDEXED

WEB OF SCIENCE™

Selection of our books indexed in the Book Citation Index in Web of Science™ Core Collection (BKCI)

Interested in publishing with us?
Contact book.department@intechopen.com

Numbers displayed above are based on latest data collected.
For more information visit www.intechopen.com

Chapter

A New BEM for Modeling of Acoustic Wave Propagation in Three-Temperature Nonlinear Generalized Magneto-Thermoelastic ISMFGA Structures Using Laser Ultrasonics

Mohamed Abdelsabour Fahmy

Abstract

The principal aim of this chapter is to introduce a new theory called acoustic wave propagation of three-temperature nonlinear generalized magneto-thermoelasticity, and we propose a new boundary element model for solving problems of initially stressed multilayered functionally graded anisotropic (ISMFGA) structures using laser ultrasonics, which connected with the proposed theory. Since there are no available analytical or numerical solutions for the considered nonlinear wave propagation problems in the literature, we propose a new boundary element modeling formulation for the solution of such problems. The numerical results are depicted graphically to show the propagation of three temperatures and displacement waves. The results also show the effects of initial stress and functionally graded material on the displacement waves and confirm the validity and accuracy of our proposed theory and solution technique.

Keywords: boundary element method, acoustic wave propagation, three-temperature, nonlinear generalized magneto-thermoelasticity, initially stressed multilayered functionally graded anisotropic structures, laser ultrasonics

1. Introduction

Physically, according to particle motion orientation and energy direction, there are three wave types, which are categorized as mechanical waves, electromagnetic waves, and matter waves. Mechanical waves are waves, which cannot travel through a vacuum and can travel through any medium at a wave speed, which depends on elasticity and inertia. There are three types of mechanical waves: longitudinal, transverse, and surface waves. Longitudinal waves occur when the movement of the particles is parallel to the energy motion like sound waves and pressure waves. Transverse waves appear when the movement of the particles is

IntechOpen

perpendicular to the energy motion like light waves, polarized waves, and electromagnetic waves. Surface waves happen when the movement of the particles is in a circular motion. These waves usually occur at interfaces like ocean waves and cup of water ripples. Electromagnetic waves are generated by a fusion of electric and magnetic fields. These waves travel through a vacuum and do not need a medium to travel like microwaves, X-ray, radio waves, and ultraviolet waves. The matter has a wave–particle duality property, where in 1905, Albert Einstein introduced a quantum mechanics theory stating that light has a dual nature; when the light is moving, it shows the wave properties, and when it is at rest, it shows the particle properties, where each light particle has an energy quantum called a photon. Sound is a pressure variation, where a condensation is an increased pressure region on a sound wave and a dilation is a decreased pressure region on a sound wave. Acoustics is the science of study related to the study of sound in gases, liquids, and solids including subjects such as vibration, sound, ultrasound, and infrasound and has grown to encompass the realm of ultrasonics and infrasonics in addition to the audio range, as the result of applications in oceanology, materials science, medicine, dentistry, communications, industrial processes, petroleum and mineral prospecting, music and voice synthesis, marine navigation, animal bioacoustics, and noise cancelation. There are two mechanisms that have been proposed to explain wave generation, which depend on the energy density of laser pulse, a first mechanism at high-energy density, where a thin layer of solid material melts, followed by a dissolution process where the particles fly off the surface, which leads to forces that generate ultrasound, and a second mechanism at low-energy density, where irradiation of laser pulses onto a material generates elastic waves due to the thermoelastic process of expansion of a surface at a high rate. Ultrasound generation with lasers offers a number of advantages over conventional generation with piezoelectric transducers. Since the ultrasound generation by a laser pulse in the thermoelastic range does not damage the material surface, it has several applications such as fiber-optic communication, narrow-band and broadband systems, the ability to work on hard to reach places, curved and rough surfaces, absolute beam energy measurements, and digital images having higher spatial resolution. The process of converting a laser source into an equivalent set of stress boundary conditions takes the largest share of the effort involved in modeling of laser-generated ultrasound, which is very useful in describing the features of a laser-generated ultrasonic in the thermoelastic system [1–3]. Due to the interaction between laser light and a metal surface, the generation of high-frequency acoustic pulses causes the laser irradiation of a metal surface. It led to great progress to develop theoretical models to describe the experimental data [4]. Scruby et al. [5] demonstrated that the thermoelastic area source has been reduced to a point-source influential on the surface. This source point ignores the optical absorption of laser energy into the bulk material and the thermal diffusion from the heat source. Moreover, it does not take into account the limited side dimensions of the source. Rose [6] introduced surface center of expansion (SCOE) based on point-source representation. The SCOE models predict the major features of laser-generated ultrasound waves and agree with experiments particularly well for highly focused Q-switched laser pulses. It fails to predict a precursor in ultrasonic waveforms on and near the epicenter. The precursor is a small sharp initial spike observed in metals signaling the arrival of the longitudinal wave. Doyle [7] established that the existence of the metal precursor is due to subsurface sources which arise from thermal diffusion, since the optical absorption depth is very small in comparison to the thermal diffusion length. According to McDonald [8], Spicer [9] used the generalized thermoelasticity theory to constitute a real model, taking into consideration spatial–temporal shape of the laser pulse and the effect of thermal diffusion.

The mathematical foundations of three-temperature thermoelasticity were defined for the first time by Fahmy [10–14]. Analytical solutions for the current nonlinear generalized thermoelastic problems which are associated with the proposed theory are very difficult to obtain, so many numerical methods were developed for solving such problems like finite difference method [15], discontinuous Galerkin method [16], finite element method (FEM) [17], boundary element method (BEM) [18–31], and other developed techniques [32–36]. The boundary element method [37–67] is actualized effectively for tackling a few designing and logical applications because of its straightforwardness, precision, and simplicity of execution.

In the present chapter, we introduce a new acoustic wave propagation theory called three-temperature nonlinear generalized magneto-thermoelasticity, and we propose a new boundary element technique for modeling problems of initially stressed multilayered functionally graded anisotropic (ISMFGA) structures using laser ultrasonics, which connected with the proposed theory, where we used the three-temperature (3T) radiative heat conduction equations combined with electron, ion, and photon temperatures in the formulation of such problems. The numerical results are presented graphically to show the effects of three temperatures on the displacement wave propagation in the x-axis direction of ISMFGA structures. The numerical results also show the propagation of the displacement waves of homogenous and functionally graded structures under the effect of initial stress. The validity and accuracy of our proposed model was demonstrated by comparing our BEM results with the corresponding FDM and FEM results.

A brief summary of the paper is as follows: Section 1 introduces the background and provides the readers with the necessary information to books and articles for a better understanding of wave propagation problems in three-temperature nonlinear generalized magneto-thermoelastic ISMFGA structures and their applications. Section 2 describes the formulation of the new theory and introduces the partial differential equations that govern its related problems. Section 3 outlines continuity and initial and boundary conditions of the considered problem. Section 4 discusses the implementation of the new BEM and its implementation for solving the governing equations of the problem to obtain the three temperatures and displacement fields. Section 5 presents the new numerical results that describe the displacement waves and three-temperature waves under the effect of initial stress on the homogeneous and functionally graded structures.

2. Formulation of the problem

Consider a multilayered structure with n functionally graded layers in the yz-plane of a Cartesian coordinate. The x-axis is the common normal to all layers as shown in **Figure 1**. The thickness of the considered multilayered structure and the ith layer is denoted by h and h^i, respectively. The considered multilayered structure which occupies the region $R = \{(x, y, z) : 0 < x < h, 0 < y < b, 0 < z < a\}$ has been placed in a primary magnetic field H_0 acting in the direction of the y-axis.

According to the three-temperature theory, the governing equations of nonlinear generalized magneto-thermoelasticity in an initially stressed multilayered functionally graded anisotropic (ISMFGA) structure for the ith layer can be written in the following form:

$$\sigma_{ab,b} + \tau_{ab,b} - \Gamma_{ab} = \rho^i (x+1)^m \ddot{u}_a^i \tag{1}$$

$$\sigma_{ab} = (\chi + 1)^m \left[C^i_{abfg} u^i_{f,g} - \beta^i_{ab} \left(T^i - T_0 + \tau_1 \dot{T}^i \right) \right] \tag{2}$$

$$\tau_{ab} = \mu^i (x + 1)^m \left(\tilde{h}_a H_b + \tilde{h}_b H_a - \delta_{ba} \left(\tilde{h}_f H_f \right) \right) \tag{3}$$

$$\Gamma_{ab} = P^i (x + 1)^m \left(\frac{\partial u^i_a}{\partial x_b} - \frac{\partial u^i_b}{\partial x_a} \right) \tag{4}$$

According to Fahmy [10], the *2D-3 T radiative heat conduction equations* can be expressed as follows:

$$\nabla \left[\left(\delta_{1j} \mathbb{K}^{i*}_\alpha + \delta_{2j} \mathbb{K}^i_\alpha \right) \nabla T^i_\alpha (r, \tau) \right] - \overline{\mathbb{W}}(r, \tau) = c^i_\alpha \rho^i \delta_1 \delta_{1j} \frac{\partial T^i_\alpha (r, \tau)}{\partial \tau} \tag{5}$$

where

$$\overline{\mathbb{W}}(r, \tau) = \begin{cases} \rho^i \mathbb{W}_{eI} \left(T^i_e - T^i_I \right) + \rho^i \mathbb{W}_{er} \left(T^i_e - T^i_p \right) + \overline{\overline{\mathbb{W}}}, \alpha = e, & \delta_1 = 1 \\ -\rho^i \mathbb{W}_{eI} \left(T^i_e - T^i_p \right) + \overline{\overline{\mathbb{W}}}, & \alpha = I, \delta_1 = 1 \\ -\rho^i \mathbb{W}_{er} \left(T^i_e - T^i_p \right) + \overline{\overline{\mathbb{W}}}, & \alpha = p, \delta_1 = T^3_p \end{cases} \tag{6}$$

in which

$$\overline{\overline{\mathbb{W}}}(r, \tau) = -\delta_{2j} \mathbb{K}^i_\alpha \dot{T}_{\alpha,ab} + \beta_{ab} T_{\alpha 0} \left[(\tau_0 + \delta_{2j}) \ddot{u}_{a,b} \right] + \rho^i c^i_\alpha \left[(\tau_0 + \delta_{1j} \tau_2 + \delta_{2j}) \ddot{T}_\alpha \right] - Q(x, \tau) \tag{7}$$

and

$$\begin{aligned} &\mathbb{W}_{eI} = \rho^i \mathbb{A}_{eI} T_e^{-2/3}, \mathbb{W}_{er} = \rho^i \mathbb{A}_{er} T_e^{-1/2}, \mathbb{K}_\alpha = \mathbb{A}_\alpha T_\alpha^{5/2}, \alpha = e, I, \\ &\mathbb{K}_p = \mathbb{A}_p T_p^{3+\mathbb{B}} \end{aligned} \tag{8}$$

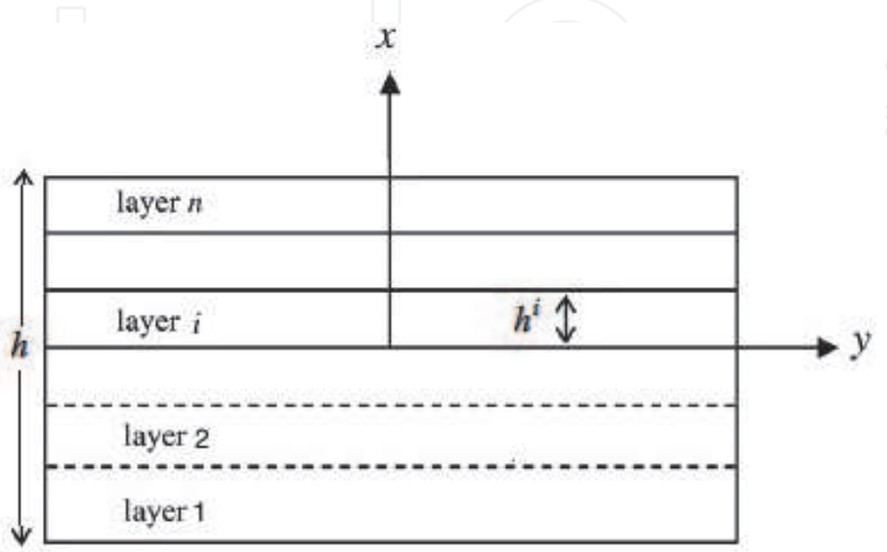

Figure 1.
Geometry of the FGA structure.

The total energy of unit mass can be described by

$$P = P_e + P_I + P_p,\ P_e = c_{\alpha e} T_e^i,\ P_I = c_{\alpha I} T_l^i,\ P_p = \frac{1}{4} c_{\alpha p} T_p^{4i} \tag{9}$$

where σ_{ab}, τ_{ab}, and u_k^i are the mechanical stress tensor, Maxwell's electromagnetic stress tensor, and displacement vector, respectively; $T_{\alpha 0}^i$ is the reference temperature; T_α^i is the temperature; C_{abfg}^i and β_{ab}^i are, respectively, the constant elastic moduli and stress-temperature coefficients of the anisotropic medium; μ^i, $\tilde{h}$, P^i, ρ^i, and c_α^i are the magnetic permeability, perturbed magnetic field, initial stress in the ith layer, density, and specific heat capacity, respectively; τ is the time; τ_0, τ_1, and τ_2 are the relaxation times; $i = 1, 2, \ldots, n-1$ represents the parameters in a multilayered structure; and m is a dimensionless constant. Also, we considered in the current study that $\tau_{ab,b} = \mu_0^i \epsilon_{abf} J_b H_f$ is the a-component of the Lorentz force and $J(\tau) = \frac{J_0 \tau}{\tau_3^2} e^{\frac{\tau}{\tau_3}}$ is the temporal profile of a non-Gaussian laser pulse, J_0 is the total energy intensity, and $Q(x,\tau) = \frac{1-R}{x_0} e^{\left(\frac{x_a}{x_0}\right) J(\tau)}$, $a = 1, 2, 3$ is the heat source intensity.

According to Fahmy [57], we notice that there are two special cases of the Green and Naghdi theory of type III; when $\mathbb{K}_\alpha^i \to 0$, the equations of GN III theory are reduced to the GN theory type II, and when $\mathbb{K}_\alpha^{i*} \to 0$, the equations of the GN III theory are reduced to the GN theory type I.

3. Continuity and initial and boundary conditions

The continuity conditions along interfaces for the temperature, heat flux, displacement, and traction can be expressed as follows:

$$T_\alpha^i(x,z,\tau)\big|_{x=h^i} = T_\alpha^{(i+1)}(x,z_t\tau)\big|_{x=h^i} \tag{10}$$

$$q^i(x,z,\tau)\big|_{x=h^i} = q^{(i+1)}(x,z,\tau)\big|_{x=h^i} \tag{11}$$

$$u_f^i(x,z,\tau)\Big|_{x=h^i} = u_f^{(i+1)}(x,z,\tau)_{x=h^i} \tag{12}$$

$$\bar{t}_a^i(x,z,\tau)\Big|_{x=h^i} = \bar{t}_a^{(i+1)}(x,z,\tau)_{x=h^i} \tag{13}$$

where n is the total number of layers, $\bar{t}_a$ are the tractions, which are defined by $\bar{t}_a = \sigma_{ab} n_b$, and $i = 1, 2, \ldots, n-1$.

The remaining initial and boundary conditions for the current study are

$$u_f^i(x,z,0) = \dot{u}_f^i(x,z,0) = 0 \quad \text{for } (x,z) \in R \cup C \tag{14}$$

$$u_f^i(x,z,\tau) = \Psi_f(x,z,\tau) \text{ for } (x,z) \in C_3 \tag{15}$$

$$\bar{t}_a^i(x,z,\tau) = \Phi_f(x,z,\tau) \text{ for } (x,z) \in C_4, \tau > 0, \tag{16}$$

$$T_\alpha^i(x,z,0) = T_\alpha^i(x,z,0) = 0 \text{ for } (x,z) \in R \cup C \tag{17}$$

$$T_\alpha^i(x,y,\tau) = \bar{f}(x,\mathrm{y},\tau) \text{ for } (x,y) \in C_1, \quad \tau > 0 \tag{18}$$

$$q^i(x,z,\tau) = \bar{h}(x,z,\tau) \text{ for } (x,z) \in C_2, \tau > 0 \tag{19}$$

where Ψ_f, Φ_f,f, and $\overline{h}$ are suitably prescribed functions and $C = C_1 \cup C_2 = C_3 \cup C_4$, $C_1 \cap C_2 = C_3 \cap C_4 = \emptyset$.

4. BEM numerical implementation

Making use of Eqs. (2)–(4), we can write (1) as follows:

$$L_{gb}u^i_f = \rho^i \ddot{u}^i_a - \left(D_a T^i_\alpha - P^i\left(\frac{\partial u^i_b}{\partial x_a} - \frac{\partial u^i_a}{\partial x_b}\right)\right) = f_{gb} \tag{20}$$

where the inertia term $\rho\ddot{u}_a$, the temperature gradient $D_a T$, and the initial stress term are treated as the body forces.

The field equations may be expressed in the operator form as follows:

$$L_{gb}u^i_f = f_{gb}, \tag{21}$$

$$L_{ab}T^i_\alpha = f_{ab} \tag{22}$$

where the operators L_{gb}, f_{gb}, L_{ab}, and f_{ab} are as follows:

$$L_{gb} = D_{abf}\frac{\partial}{\partial x_b} + D_{af} + \Lambda D_{a1f}, \qquad L_{ab} = \left(\delta_{2j}\mathbb{K}^{i*}_\alpha\right)\nabla \tag{23}$$

$$f_{gb} = \rho^i \ddot{u}^i_a - \left(D_a T^i_\alpha - P^i\left(\frac{\partial u^i_b}{\partial x_a} - \frac{\partial u^i_a}{\partial x_b}\right)\right) \tag{24}$$

$$f_{ab} = \nabla\left(\delta_{1j}\mathbb{K}^i_\alpha\right)\nabla + \rho^i c^i_\alpha \delta_1 \delta_{1j}(x+1)^m \dot{T}^i_\alpha + \overline{\mathbb{W}}(r,\tau) \tag{25}$$

where

$$D_{abf} = C_{abfg}\varepsilon, \varepsilon = \frac{\partial}{\partial x_g}, D_{af} = \mu H_0^2\left(\frac{\partial}{\partial x_a} + \delta_{a1}\Lambda\right)\frac{\partial}{\partial x_f},$$
$$D_a = -\beta^i_{ab}\left(\frac{\partial}{\partial x_b} + \delta_{b1}\Lambda + \tau_1\left(\frac{\partial}{\partial x_b} + \Lambda\right)\frac{\partial}{\partial \tau}\right), \quad \Lambda = \frac{m}{x+1}.$$

The differential equation (21) can be solved using the weighted residual method (WRM) to obtain the following integral equation:

$$\int_R \left(L_{gb}u^i_f - f_{gb}\right)u^{i*}_{da}dR = 0 \tag{26}$$

Now, the fundamental solution u^{i*}_{df} and traction vectors t^{i*}_{da} and t^i_a can be written as follows:

$$L_{gb}u^{i*}_{af} = -\delta_{ad}\delta(x,\xi) \tag{27}$$

$$t^{i*}_{da} = C_{abfg}u^{i*}_{df,g}n_b \tag{28}$$

$$t^i_a = \frac{\overline{t}^i_a}{(x+1)^m} = \left(C_{abfg}u^i{}_{f,g} - \beta^i_{ab}\left(T^i_\alpha + \tau_1 T^i_\alpha\right)\right)n_b \tag{29}$$

Using integration by parts and sifting property of the Dirac distribution for (26), then using Eqs. (27) and (29), we can write the following elastic integral representation formula:

$$u_d^i(\xi) = \int_C \left(u_{da}^{i*} t_a^i - t_{da}^{i*} u_a^i + u_{da}^{i*} \beta_{ab}^i T_\alpha^i n_b\right) dC - \int_R f_{gb} u_{da}^{i*} dR \tag{30}$$

The fundamental solution T^{i^*} can be defined as

$$L_{ab} T^{i^*} = -\delta(x, \xi) \tag{31}$$

By using WRM and integration by parts, we can write (23) as follows:

$$\int_R \left(L_{ab} T_\alpha^i T_\alpha^{i^*} - L_{ab} T_\alpha^{i^*} T_\alpha^i\right) dR = \int_C \left(q^{i^*} T_\alpha^i - q^i T_\alpha^{i^*}\right) dC \tag{32}$$

where

$$q^i = -\mathbb{K}_\alpha^i T_{\alpha.b}^i n_a \tag{33}$$

$$q^{i*} = -\mathbb{K}_\alpha^i T_{\alpha,b}^{i^*} n_a \tag{34}$$

By the use of sifting property, we obtain from (32) the thermal integral representation formula:

$$T_\alpha^i(\xi) = \int_C \left(q^{i^*} T_\alpha^i - q^i T_\alpha^{i^*}\right) dC - \int_R f_{ab} T_\alpha^{i^*} dR \tag{35}$$

By combining (30) and (35), we have

$$\begin{bmatrix} u_d^i(\xi) \\ T_\alpha^i(\xi) \end{bmatrix} = \int_C \left\{ -\begin{bmatrix} t_{da}^{i*} & -u_{aa}^{i*} \beta_{ab} n_b \\ 0 & -q^{i*} \end{bmatrix} \begin{bmatrix} u_a^i \\ T_\alpha^i \end{bmatrix} + \begin{bmatrix} u_{da}^{i*} & 0 \\ 0 & -T_\alpha^{i*} \end{bmatrix} \begin{bmatrix} \tau_a^i \\ q^i \end{bmatrix} \right\} dC - \int_R \begin{bmatrix} u_{da}^{i*} & 0 \\ 0 & -T_\alpha^{i*} \end{bmatrix} \begin{bmatrix} f_{gb} \\ -f_{ab} \end{bmatrix} dR \tag{36}$$

The generalized thermoelastic vectors can be expressed in contracted notation form as follows:

$$U_A^i = \begin{cases} u_a^i & a = A = 1, 2, 3 \\ T_\alpha^i & A = 4 \end{cases} \tag{37}$$

$$\mathrm{T}_{\alpha A}^i = \begin{cases} t_a^i & a = A = 1, 2, 3 \\ q^i & A = 4 \end{cases} \tag{38}$$

$$U_{DA}^{i*} = \begin{cases} u_{da}^{i*} & d = D = 1, 2, 3; a = A = 1, 2, 3 \\ 0 & d = D = 1, 2, 3; A = 4 \\ 0 & D = 4; a = A = 1, 2, 3 \\ -T_\alpha^{i*} & D = 4; A = 4 \end{cases} \tag{39}$$

$$\tilde{T}_{\alpha DA}^{i^*} = \begin{cases} t_{aa}^{i*} & d = D = 1, 2, 3; a = A = 1, 2, 3 \\ -\tilde{u}_d^{i*} & d = D = 1, 2, 3; A = 4 \\ 0 & D = 4; a = A = 1, 2, 3 \\ -q^{i*} & D = 4; A = 4 \end{cases} \tag{40}$$

$$\tilde{u}_d^{i*} = u_{da}^{i*}\beta_{af}^i n_f \tag{41}$$

Using the previous vectors, we can write (36) as

$$U_D^i(\xi) = \int_C \left(U_{DA}^{i*}\mathrm{T}_{\alpha A}^i - \tilde{T}_{\alpha DA}^i U_A^i\right)dC - \int_R U_{DA}^{i*} S_A dR \tag{42}$$

The vector S_A can be split as follows

$$S_A = S_A^0 + S_A^T + S_A^{\mathrm{u}} + S_A^{\dot{T}} + S_A^{\ddot{T}} + S_A^{\ddot{u}} \tag{43}$$

where

$$S_A^0 = \begin{cases} 0 & A = 1,2,3 \\ \dfrac{1-R}{x_0} e^{\left(-\frac{x_a}{x_0}\right)J(\tau)} & A = 4 \end{cases} \tag{44}$$

$$S_A^T = \omega_{AF} U_F^i \text{with} \omega_{AF} = \begin{cases} -D_a & A = 1,2,3; F = 4 \\ \nabla\left(\delta_{2j}\mathbb{K}_\alpha^{i^*}\right)\nabla & \text{otherwise} \end{cases} \tag{45}$$

$$S_A^u = \psi U_F^i \text{with} \psi = \begin{cases} P^i\left(\dfrac{\partial}{\partial xb} - \dfrac{\partial}{\partial x_a}\right) & A = 1,2,3; F = 1,2,3, \\ 0 & A = 4; F = 4 \end{cases} \tag{46}$$

$$S_A^{\dot{T}} = \Gamma_{AF}\dot{U}_F^i \quad \text{with} \quad \Gamma_{AF} = \begin{cases} -\beta_{ab}^i \tau_1\left(\dfrac{\partial}{\partial x_b} + \Lambda\right)\dfrac{\partial}{\partial \tau} & A = 4; F = 4 \\ \rho^i c_\alpha^i \delta_1 \delta_{1j} & \text{otherwise} \end{cases} \tag{47}$$

$$S_A^{\ddot{T}} = \delta_{AF}\ddot{U}_F^i \ \text{ with } \ \delta_{AF} = \begin{cases} 0 & A = 4; F = 4 \\ \rho^i c_\alpha^i\left[\left(\tau_0 + \delta_{1j}\tau_2 + \delta_{2j}\right)\right] & \text{otherwise} \end{cases} \tag{48}$$

$$S_A^{\ddot{\mathrm{u}}} = \tilde{\sigma}\ddot{U}_F^i \ \text{ with } \ \tilde{\sigma} = \begin{cases} \rho^i & A = 1,2,3, F = 1,2,3, \\ \beta_{ab}^i T_{\alpha 0}^i(\tau_0 + \delta_{2i}) & A = 4; F = 4 \end{cases} \tag{49}$$

The thermoelastic representation formula (36) can also be written in matrix form as follows:

$$\begin{aligned}[S_A] = &-\begin{bmatrix} 0 \\ -\dfrac{1-R}{x_0} \quad e\left(-\dfrac{x_a}{x_0}\right)J(\tau) \end{bmatrix} + \left\{\begin{bmatrix} -D_a T_\alpha^i \\ \nabla\left(\delta_{2j}\mathbb{K}_\alpha^{i^*}\right)\nabla T_\alpha^i \end{bmatrix}\right\} + \begin{bmatrix} P^i\left(u_{b,a}^{i_0} - u_{a,b}^i\right) \\ 0 \end{bmatrix} \\ &+ \begin{bmatrix} -\beta_{ab}^i \tau_1\left(\dfrac{\partial}{\partial x_b} + \Lambda\right)\dot{T}_\alpha^i \\ \rho^i c_\alpha^i \delta_1 \delta_{1j}\dot{T}_\alpha^i \end{bmatrix} + \rho^i c_\alpha^i\left[\left(\tau_0 + \delta_{1j}\tau_2 + \delta_{2j}\right)\right]\begin{bmatrix} 0 \\ \ddot{T}_\alpha^i \end{bmatrix} \\ &+ \begin{bmatrix} \rho^i \ddot{u}_a^i \\ \beta_{ab}^i T_{\alpha 0}^i\left(\tau_0 + \delta_{2j}\right)\ddot{u}_{f,g}^i \end{bmatrix} \end{aligned} \tag{50}$$

To transform the domain integral in (42) to the boundary, we approximate the source vector S_A by a series of given tensor functions f_{AE}^q and unknown coefficients α_E^q as follows:

$$S_A \approx \sum_{q=1}^{E} f_{AE}^{q} \alpha_E^q \tag{51}$$

Thus, the thermoelastic representation formula (42) can be written in the following form:

$$U_D(\xi) = \int_C \left(U_{DA}^{i^*} T_{\alpha A}^{i} - \tilde{T}_{\alpha DA}^{i^*} U_A^i \right) dC - \sum_{q=1}^{N} \int_R U_{DA}^{i^*} f_{AE}^{q} dR\, \alpha_E^q \tag{52}$$

By implementing the WRM to the following equations.

$$L_{gb} u_{fe}^{iq} = f_{ae}^{q} \tag{53}$$

, $$L_{ab} T_{\alpha}^{iq} = f_{pj}^{q} \tag{54}$$

Then, the elastic and thermal representation formulae are given as follows [46]:

$$u_{de}^{iq}(\xi) = \int_C \left(u_{da}^{i*} t_{ae}^{iq} - t_{da}^{i*} u_{ae}^{iq} \right) dC - \int_R u_{da}^{i*} f_{ae}^{q} dR \tag{55}$$

$$T_{\alpha}^{iq}(\xi) = \int_C \left(q^{i*} T_{\alpha}^{iq} - q^{iq} T_{\alpha}^{i*} \right) dC - \int_R f^{q} T_{\alpha}^{i*} dR \tag{56}$$

The representation formulae (55) and (56) can be combined into the following single equation:

$$U_{DE}^{iq}(\xi) = \int_C \left(U_{DA}^{i*} T_{\alpha AE}^{iq} - T_{\alpha DA}^{i*} U_{AE}^{iq} \right) dC - \int_R U_{DA}^{i*} f_{AE}^{iq} dR \tag{57}$$

With the substitution of (57) into (52), the dual reciprocity representation formula of coupled thermoelasticity can be expressed as follows:

$$\begin{aligned} U_D^i(\xi) = & \int_C \left(U_{DA}^{i*} T_{\alpha A}^{i} - \breve{T}_{\alpha DA}^{i*} U_A^i \right) dC \\ & + \sum_{q=1}^{E} \left(U_{DE}^{iq}(\xi) + \int_C \left(T_{\alpha DA}^{i*} U_{AE}^{iq} - U_{DA}^{i*} T_{\alpha AE}^{iq} \right) dC \right) \alpha_E^q \end{aligned} \tag{58}$$

To calculate interior stresses, (58) is differentiated with respect to ξ_l as follows:

$$\begin{aligned} \frac{\partial U_D^i(\xi)}{\partial \xi_l} = & -\int_C \left(U_{DA,l}^{i*} T_{\alpha A,l}^{i} - \breve{T}_{\alpha DA,l}^{i^*} U_A^i \right) dC \\ & + \sum_{q=1}^{E} \left(\frac{\partial U_{DE}^{iq}(\xi)}{\partial \xi_l} - \int_C \left(T_{\alpha DA,l}^{i*} U_{\alpha AE}^{iq} - U_{DA,l}^{i*} T_{\alpha AE}^{iq} \right) dC \right) \alpha_E^q \end{aligned} \tag{59}$$

According to the dual reciprocity boundary integral equation procedure of Fahmy [44], we can write (58) in the following system of equations:

$$\breve{\zeta}U - \eta T_\alpha = \left(\zeta\breve{U} - \eta\breve{\wp}\right)\alpha \tag{60}$$

The generalized displacements and velocities are approximated in terms of a series of known tensor functions f^q_{FD} and unknown coefficients γ^q_D and $\tilde{\gamma}^q_D$:

$$U^i_F \approx \sum_{q=1}^{N} f^q_{FD}(x)\gamma^q_D \tag{61}$$

where

$$f^q_{FD} = \begin{cases} f^q_{fd} & f = F = 1,2,3; d = D = 1,2,3 \\ f^q & F = 4; D = 4 \\ 0 & \text{otherwise} \end{cases} \tag{62}$$

The gradients of the generalized displacements and velocities can also be approximated in terms of the derivatives of tensor functions as follows:

$$U^i_{F,g} \approx \sum_{q=1}^{N} f^q_{FD,g}(x)\gamma^q_K \tag{63}$$

These approximations are substituted into Eq. (45) to obtain

$$S^T_A = \sum_{q=1}^{N} S_{AF} f^q_{FD,g}\gamma^q_D \tag{64}$$

By implementing the point collocation procedure introduced by Gaul et al. [43] to Eqs. (51) and (61), we have

$$\breve{S} = J\overline{\alpha}, \quad U^i = J'\gamma, \tag{65}$$

Similarly, the implementation of the point collocation procedure to Eqs. (64), (46), (47), (48), and (49) leads to the following equations:

$$\breve{S}^{T^i_\alpha} = \mathcal{B}^T\gamma \tag{66}$$

$$S^u_A = \overline{\psi}U^i \tag{67}$$

$$\breve{S}^{\dot{T}^j_\alpha} = \overline{\Gamma}_{AF}\dot{U}^i \tag{68}$$

$$\breve{S}^{\ddot{T}^j_\alpha} = \overline{\delta}_{AF}\ddot{U}^i \tag{69}$$

$$\breve{S}^{\ddot{u}} = \overline{\tilde{\sigma}}\ddot{U}^i \tag{70}$$

where $\overline{\psi}$, $\overline{\Gamma}_{AF}$, $\overline{\delta}_{AF}$, and $\overline{\tilde{\sigma}}$ are assembled using the submatrices $[\psi]$, $[\Gamma_{AF}]$, $[\delta_{AF}]$, and $[\tilde{\sigma}]$, respectively.

Solving the system (65) for α and γ yields

$$\overline{\alpha} = J^{-1}\breve{S}, \quad \gamma = J'^{-1}U^i \tag{71}$$

Now, the coefficients α can be expressed in terms of nodal values of the unknown displacements U^i, velocities $\dot{U}^i$, and accelerations $\ddot{U}^i$ as follows:

$$\overline{\alpha} = J^{-1}\left(\breve{S}^0 + \left(\mathcal{B}^T J'^{-1} + \overline{\psi}\right]U^i + \overline{\Gamma}_{AF}\dot{U}^i + \left(\overline{\delta} + \overline{\delta}_{AF}\right)\ddot{U}^i\right) \tag{72}$$

An implicit-implicit staggered algorithm for the integration of the governing equations was developed and implemented for use with the DRBEM for solving the governing equations which may now be written in a more convenient form after substitution of Eq. (72) into Eq. (60) as follows:

$$\widehat{M}\ddot{U}^i + \widehat{\Gamma}\dot{U}^i + \widehat{K}U^i = \widehat{\mathbb{Q}}^i \tag{73}$$

$$\widehat{\mathrm{X}}\ddot{T}^i_\alpha + \widehat{\mathrm{A}}\dot{T}^i_\alpha + \widehat{\mathrm{B}}T^i_\alpha = \widehat{\mathbb{Z}}\ddot{U}^i + \widehat{\mathbb{R}} \tag{74}$$

where $V = \left(\eta\breve{\wp} - \zeta\breve{U}\right)J^{-1}$, $\widehat{M} = V\left(\overline{\delta} + \overline{\delta}_{AF}\right)$, $\widehat{\Gamma} = V\overline{\Gamma}_{AF}$,
$\widehat{K} = -\breve{\zeta} + V\left(\mathcal{B}^T J\prime^{-1} + \overline{\psi}\right)$, $\widehat{\mathbb{Q}}^i = -\eta\breve{T} + V\breve{S}^0$, $\widehat{\mathrm{X}} = -\rho^i c^i (x+1)^m$,
$\widehat{\mathrm{A}} = k^i_{ab}\frac{\partial}{\partial x_a}\frac{\partial}{\partial x_b}$, $\widehat{\mathrm{B}} = k^{i^*}_{ab}\frac{\partial}{\partial x_a}\frac{\partial}{\partial x_b}$, $\widehat{\mathbb{Z}} = \beta^i_{ab}T_0$, $\widehat{\mathbb{R}} = -\frac{1-R}{x_0}e^{\left(\frac{x_a}{x_0}\right)J(\tau)}$

where V, $\widehat{M}$, $\widehat{\Gamma}$, $\widehat{K}$, $\widehat{\mathrm{A}}$, and $\widehat{\mathrm{B}}$ represent the volume, mass, damping, stiffness, capacity, and conductivity matrices, respectively, and $\ddot{U}^i$, $\dot{U}^i$, U^i, T^i, and $\widehat{\mathbb{Q}}^i$ represent the acceleration, velocity, displacement, temperature, and external force vectors, respectively.

In many applications, the coupling term $\widehat{\mathbb{Z}}\ddot{U}^i_{n+1}$ that appears in the heat conduction equation and which is induced by the effect of the strain rate is negligible.

Hence, Eqs. (73) and (74) lead to the following coupled system of differential-algebraic equations (DAEs):

$$\widehat{M}\ddot{U}^i_{n+1} + \widehat{\Gamma}\dot{U}^i_{n+1} + \widehat{K}U^i_{n+1} = \widehat{\mathbb{Q}}^{ip}_{n+1} \tag{75}$$

$$\widehat{\mathrm{X}}\ddot{T}^i_{\alpha(n+1)} + \widehat{\mathrm{A}}\dot{T}^i_{\alpha(n+1)} + \widehat{\mathrm{B}}T^i_{\alpha(n+1)} = \widehat{\mathbb{Z}}\ddot{U}^i_{n+1} + \widehat{\mathbb{R}} \tag{76}$$

where $\widehat{\mathbb{Q}}^{ip}_{n+1} = \eta T^{ip}_{\alpha(n+1)} + V\breve{S}^0$ and $T^{ip}_{\alpha(n+1)}$ is the predicted temperature.

Integrating Eq. (73) with the use of trapezoidal rule and Eq. (75), we obtain

$$\begin{aligned} U^i_{n+1} &= \dot{U}^i_n + \frac{\Delta\tau}{2}\left(\ddot{U}^i_{n+1} + \ddot{U}^i_n\right) \\ &= \dot{U}^i_n + \frac{\Delta\tau}{2}\left[\ddot{U}^i_n + \widehat{M}^{-1}\left(\widehat{\mathbb{Q}}^{ip}_{n+1} - \widehat{\Gamma}\dot{U}^i_{n+1} - \widehat{K}U^i_{n+1}\right)\right] \end{aligned} \tag{77}$$

$$\begin{aligned} U^i_{n+1} &= U^i_n + \frac{\Delta\tau}{2}\left(\dot{U}^i_{n+1} + \dot{U}^i_n\right) \\ &= U^i_n + \Delta\tau\dot{U}^i_n + \frac{\Delta\tau^2}{4}\left[\ddot{U}^i_n + \widehat{M}^{-1}\left(\tilde{\mathbb{Q}}^{ip}_{n+1} - \widehat{\Gamma}\dot{U}^i_{n+1} - \widehat{K}U^i_{n+1}\right)\right] \end{aligned} \tag{78}$$

From Eq. (77) we have

$$\dot{U}^i_{n+1} = \overline{\Upsilon}^{-1}\left[\dot{U}^i_n + \frac{\Delta\tau}{2}\left[\ddot{U}^i_n + \widehat{M}^{-1}\left(\widehat{\mathbb{Q}}^{ip}_{n+1} - \widehat{K}U^i_{n+1}\right)\right]\right] \tag{79}$$

where $\overline{\Upsilon} = \left(I + \frac{\Delta\tau}{2}\widehat{M}^{-1}\widehat{\Gamma}\right)$.

Substituting from Eq. (79) into Eq. (78), we derive

$$\begin{aligned} U^i_{n+1} = U^i_n + \Delta\tau\dot{U}^i_n + \frac{\Delta\tau^2}{4}\Bigg[\ddot{U}^i_n + \widehat{M}^{-1}\Bigg(\tilde{\mathbb{Q}}^{ip}_{n+1} - \widehat{\Gamma}\overline{\Upsilon}^{-1} \\ \left[\dot{U}^i_n + \frac{\Delta\tau}{2}\right]\left[\ddot{U}^i_n + \widehat{M}^{-1}\left(\widehat{\mathbb{Q}}^{ip}_{n+1} - \widehat{K}U^i_{n+1}\right)\right] - \widehat{K}U^i_{n+1}\Bigg)\Bigg] \end{aligned} \tag{80}$$

Substituting $\dot{U}^i_{n+1}$ from Eq. (79) into Eq. (75), we obtain

$$\ddot{U}^i_{n+1} = \widehat{M}^{-1}\left[\widehat{\mathbb{Q}}^{ip}_{n+1} - \widehat{\Gamma}\left[\overline{\Upsilon}^{-1}\left[\dot{U}^i_n + \frac{\Delta\tau}{2}\left[\ddot{U}^i_n + \widehat{M}^{-1}\left(\widehat{\mathbb{Q}}^{ip}_{n+1} - \widehat{K}U^i_{n+1}\right)\right]\right]\right] - \widehat{K}U^i_{n+1}\right] \tag{81}$$

Integrating the heat Eq. (74) using the trapezoidal rule and Eq. (76), we get

$$\begin{aligned} \dot{T}^i_{\alpha(n+1)} &= \dot{T}^i_n + \frac{\Delta\tau}{2}\left(\ddot{T}^i_{\alpha(n+1)} + \ddot{T}^i_{\alpha n}\right) \\ &= \dot{T}^i_{\alpha n} + \frac{\Delta\tau}{2}\left(\widehat{\mathrm{X}}^{-1}\left[\widehat{\mathbb{Z}}\ddot{U}^i_{n+1} + \widehat{\mathbb{R}} - \widehat{\mathrm{A}}\dot{T}^{i^{\mathrm{A}}}_{\alpha(n+1)} - \widehat{\mathrm{B}}T^i_{\alpha(n+1)}\right] + \ddot{T}^i_{\alpha n}\right) \end{aligned} \tag{82}$$

$$\begin{aligned} T^i_{\alpha(n+1)} &= T^i_{\alpha n} + \frac{\Delta\tau}{2}\left(\dot{T}^i_{\alpha(n+1)} + \dot{T}^i_{\alpha n}\right) \\ &= T^i_{\alpha n} + \Delta\tau\dot{T}^i_{\alpha n} \\ &\quad + \frac{\Delta\tau^2}{4}\left(\ddot{T}^i_{\alpha n} + \widehat{\mathrm{X}}^{-1}\left[\widehat{\mathbb{Z}}\ddot{U}^i_{n+1} + \widehat{\mathbb{R}} - \widehat{\mathrm{A}}\dot{T}^i_{\alpha(n+1)} - \widehat{\mathrm{B}}T^i_{\alpha(n+1)}\right]\right) \end{aligned} \tag{83}$$

From Eq. (82) we get

$$\dot{T}^i_{\alpha(n+1)} = \Upsilon^{-1}\left[\dot{T}^i_{\alpha n} + \frac{\Delta\tau}{2}\left(\widehat{\mathrm{X}}^{-1}\left[\widehat{\mathbb{Z}}\ddot{U}^i_{n+1} + \widehat{\mathbb{R}} - \widehat{\mathrm{B}}T^i_{\alpha(n+1)}\right] + \ddot{T}^i_{\alpha n}\right)\right] \tag{84}$$

where $\Upsilon = \left(I + \frac{1}{2}\widehat{\mathrm{A}}\Delta\tau\widehat{\mathrm{X}}^{-1}\right)$

Substituting from Eq. (84) into Eq. (83), we have

$$\begin{aligned} T^i_{\alpha(n+1)} = T^i_{\alpha n} + \Delta\tau\dot{T}^i_{\alpha n} + \frac{\Delta\tau^2}{4}\Bigg(\ddot{T}^i_{\alpha n} + \widehat{\mathrm{X}}^{-1}\Bigg[\widehat{\mathbb{Z}}\ddot{U}^i_{n+1} + \widehat{\mathbb{R}} - \widehat{\mathrm{A}}\Big(\mathrm{Y}^{-1}\left[\dot{T}^i_{\alpha n}\right] \\ + \frac{\Delta\tau}{2}\left(\widehat{\mathrm{X}}^{-1}\left[\widehat{\mathbb{Z}}\ddot{U}^i_{n+1} + \widehat{\mathbb{R}} - \widehat{\mathrm{B}}T^i_{\alpha(n+1)}\right] + \ddot{T}^i_{\alpha n}\right)\Big) - \tilde{\mathrm{B}}T^i_{\alpha(n+1)}\Bigg]\Bigg) \end{aligned} \tag{85}$$

Substituting $\dot{T}^{i}_{n+1}$ from Eq. (84) into Eq. (76), we obtain

$$\ddot{T}_{\alpha(n+1)}\dot{\imath}^{\mathrm{A}} = \widehat{\mathrm{X}}^{-1}\left[\widehat{\mathbb{Z}}\ddot{U}^{i}_{n+1} + \widehat{\mathbb{R}} - \widehat{\mathrm{A}}\left(\Upsilon^{-1}\left[\dot{T}^{i}_{\alpha n} + \frac{\Delta\tau}{2}\left(\widehat{\mathrm{X}}^{-1}\right.\right.\right.\right.$$
$$\left.\left.\left.\left.\left[\widehat{\mathbb{Z}}\ddot{U}^{i}_{n+1} + \widehat{\mathbb{R}} - \widehat{\mathrm{B}}T^{i}_{\alpha(n+1)}\right] + \ddot{T}^{i}_{\alpha(n+1)}\right)\right]\right) - * \widehat{\mathrm{B}}T^{i}_{\alpha(n+1)}\right] \tag{86}$$

Now, a displacement-predicted staggered procedure for the solution of (80) and (85) is as follows:

The first step is to predict the propagation of the displacement wave field: $U^{ip}_{n+1} = U^{i}_{n}$. The second step is to substitute $\dot{U}^{i}_{n+1}$ and $\ddot{U}^{i}_{n+1}$ from Eqs. (77) and (75), respectively, in Eq. (85) and solve the resulting equation for the three-temperature wave fields. The third step is to correct the displacement wave propagation using the computed three-temperature fields for Eq. (80). The fourth step is to compute $\dot{U}^{i}_{n+1}$, $\ddot{U}^{i}_{n+1}$, $\dot{T}^{i}_{\alpha(n+1)}$, and $\ddot{T}^{i}_{\alpha(n+1)}$ from Eqs. (79), (81), (82), and (86), respectively.

5. Numerical results and discussion

In order to show the numerical results of this study, we consider a monoclinic graphite-epoxy as an anisotropic thermoelastic material which has the following physical constants [57]:

The elasticity tensor is expressed as

$$C_{pjkl} = \begin{bmatrix} 430.1 & 130.4 & 18.2 & 0 & 0 & 201.3 \\ 130.4 & 116.7 & 21.0 & 0 & 0 & 70.1 \\ 18.2 & 21.0 & 73.6 & 0 & 0 & 2.4 \\ 0 & 0 & 0 & 19.8 & -8.0 & 0 \\ 0 & 0 & 0 & -8.0 & 29.1 & 0 \\ 201.3 & 70.1 & 2.4 & 0 & 0 & 147.3 \end{bmatrix} \mathrm{GPa} \tag{87}$$

The mechanical temperature coefficient is

$$\beta_{pj} = \begin{bmatrix} 1.01 & 2.00 & 0 \\ 2.00 & 1.48 & 0 \\ 0 & 0 & 7.52 \end{bmatrix} \cdot 10^{6}\,\frac{\mathrm{N}}{\mathrm{Km}^{2}} \tag{88}$$

The thermal conductivity tensor is

$$k_{pj} = \begin{bmatrix} 5.2 & 0 & 0 \\ 0 & 7.6 & 0 \\ 0 & 0 & 38.3 \end{bmatrix} \mathrm{W/Km} \tag{89}$$

Mass density $\rho = 7820\,\mathrm{kg/m^3}$ and heat capacity $c = 461\,\mathrm{J/kg\,K}$.

The proposed technique that has been utilized in the present chapter can be applicable to a wide range of laser wave propagations in three-temperature nonlinear generalized thermoelastic problems of FGA structures. The main aim of this paper was to assess the impact of three temperatures on the acoustic

displacement waves; the numerical outcomes are completed and delineated graphically for electron, ion, phonon, and total temperatures.

Figure 2 shows the three temperatures T_e, T_i, and T_p and total temperature $T(T = T_e + T_i + T_p)$ wave propagation along the x-axis. It was shown from this figure that the three temperatures are different and they may have great effects on the connected fields.

Figures 3 and **4** show the displacement u_1 and u_2 acoustic waves propagation along x-axis for the three temperatures T_e, T_i, T_p and total temperature T. It was noticed from **Figures 3** and **4** that the three temperatures and total temperature have great effects on the acoustic displacement waves.

In order to evaluate the influence of the functionally graded parameter and initial stress on the propagation of the displacement waves u_1 and u_2 along the x-axis, the numerical results are presented graphically, as shown in **Figures 5** and **6**. These results are compared for different values of initial stress parameter and functionally graded parameter according to the following cases, A, B, C, and D,

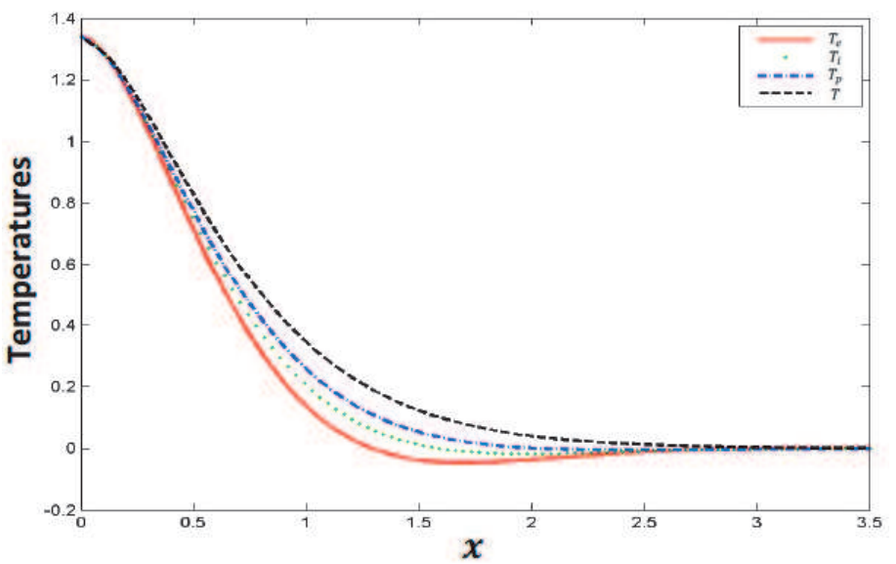

Figure 2.
Propagation of the temperature T_e, T_i, T_p *and* T *waves along the* **x**-*axis.*

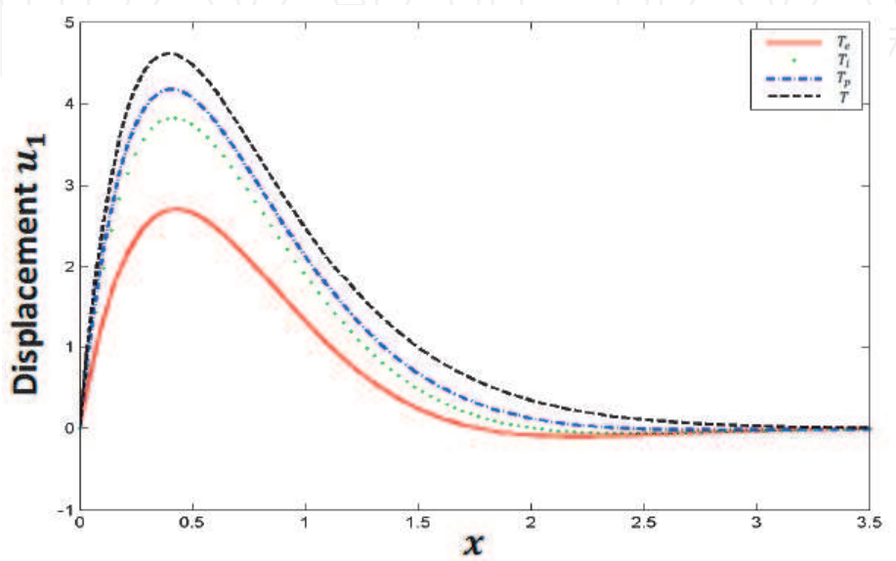

Figure 3.
Propagation of the displacement u_1 *waves along the* x-*axis.*

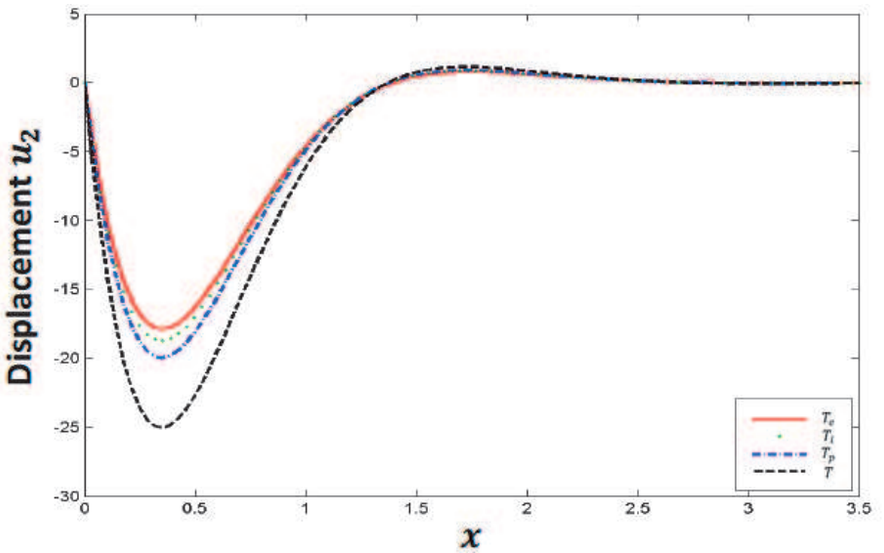

Figure 4.
Propagation of the displacement $\mathbf{u}_2$ *waves along the* $\mathbf{x}$*-axis.*

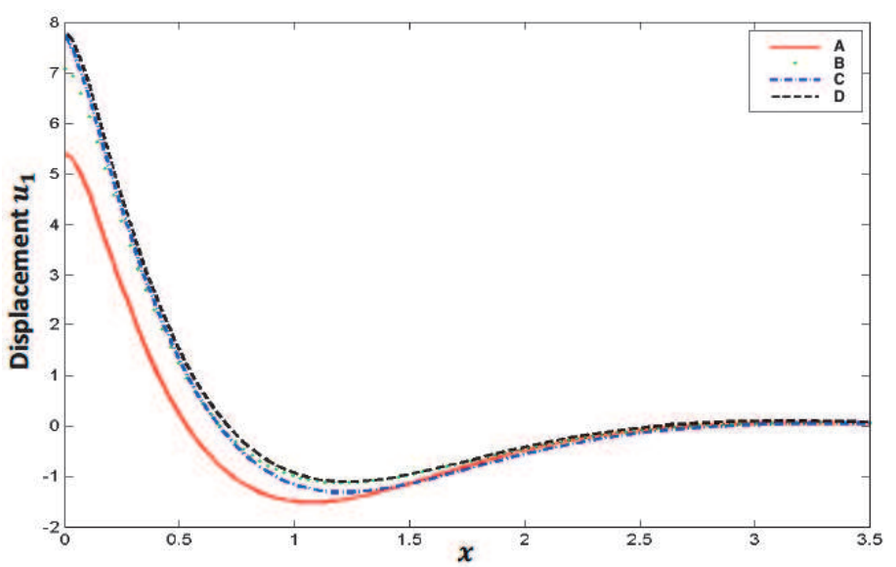

Figure 5.
Propagation of the displacement $\mathbf{u}_1$ *waves along the* $\mathbf{x}$*-axis.*

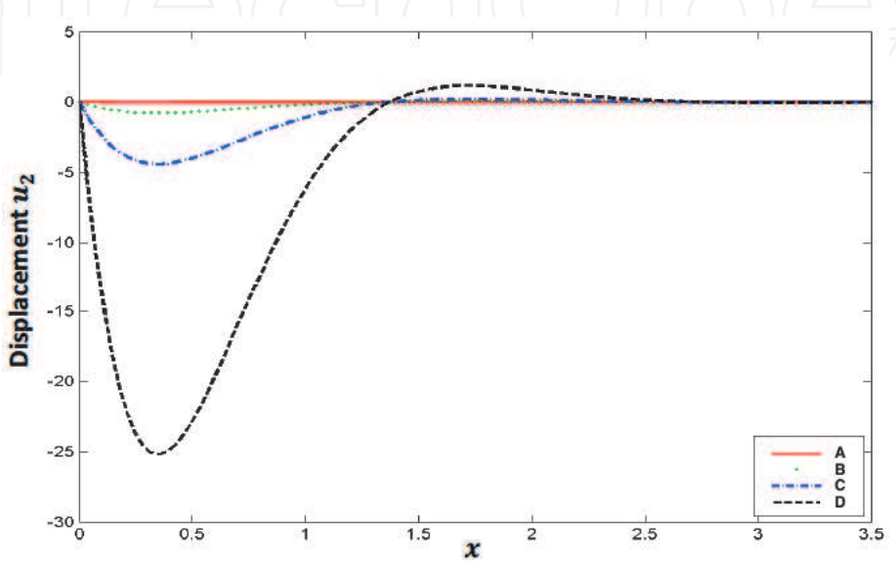

Figure 6.
Propagation of the displacement $\mathbf{u}_2$ *waves along the* $\mathbf{x}$*-axis.*

where A represents the numerical results for homogeneous ($m = 0$) structures in the absence of initial stress ($P = 0$), B represents the numerical results for functionally graded ($m = 0.5$) structures in the absence of initial stress ($P = 0$), C represents the numerical results for homogeneous ($m = 0$) structures in the presence of initial stress ($P = 0.5$), and D represents the numerical results for functionally graded ($m = 0.5$) structures in the presence of initial stress ($P = 0.5$). It can be seen from **Figures 5** and **6** that the effects of initial stress and functionally graded parameter are very pronounced.

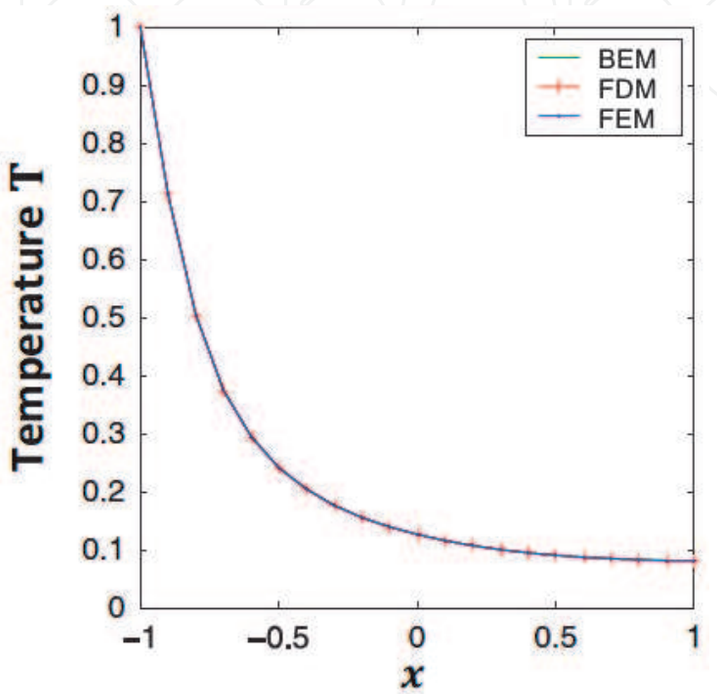

Figure 7.
Propagation of the temperature **T** *waves along the* **x***-axis for BEM, FDM, and FEM.*

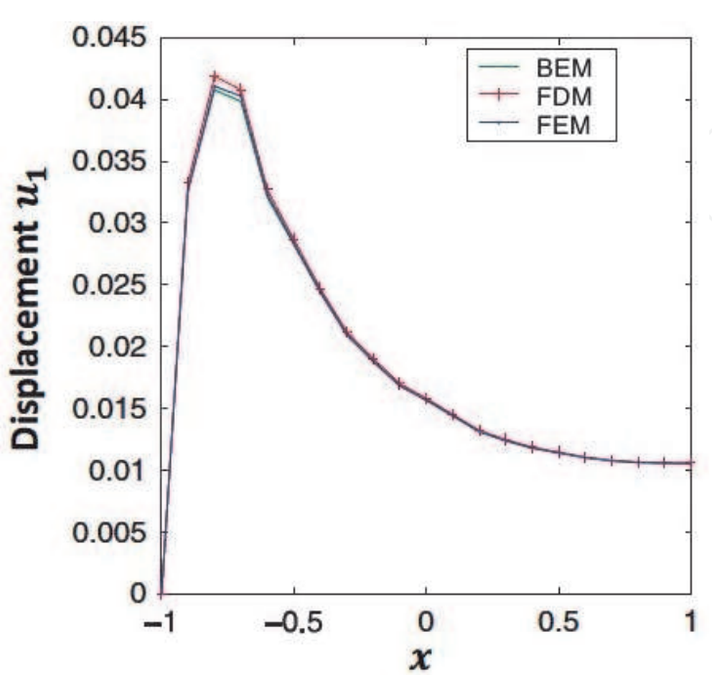

Figure 8.
Propagation of the displacement $\mathbf{u}_1$ *waves along the* **x***-axis for BEM, FDM, and FEM.*

Since there are no available results for the three-temperature thermoelastic problem, except for Fahmy's research [10–14]. For comparison purposes with the special cases of other methods treated by other authors, we only considered a one-dimensional special case of nonlinear generalized magneto-thermoelastic of anisotropic structure [11, 12] as a special case of the considered problem. In the special case under consideration, the temperature and displacement wave propagation results are plotted in **Figures 7** and **8**. The validity and accuracy of our proposed BEM technique was demonstrated by comparing graphically the BEM results for the considered problem with those obtained using the finite difference method (FDM) of Pazera and Jędrysiak [68] and finite element method (FEM) of Xiong and Tian [69] results based on replacing heat conduction with three-temperature heat conduction; it can be noticed that the BEM results are found to agree very well with the FDM or FEM results.

6. Conclusion

Propagation of displacements and temperature acoustic waves in three-temperature nonlinear generalized magneto-thermoelastic ISMFGA structures has been studied, where we used the three-temperature nonlinear radiative heat conduction equations combined with electron, ion, and phonon temperatures. The BEM results of the considered model show the differences between electron, ion, phonon, and total temperature distributions within the ISMFGA structures. The effects of electron, ion, phonon, and total temperatures on the propagation of acoustic displacement waves have been investigated. Also, the effects of functionally graded parameter and initial stress on the propagation of acoustic displacement waves have been established. Since there are no available results for comparison, except for the one-temperature heat conduction problems, we considered the one-dimensional special case of our general model based on replacing three-temperature radiative heat conductions with one-temperature heat conduction for the verification and demonstration of the considered model results. In the considered special case, the BEM results have been compared graphically with the FDM and FEM, and it can be noticed that the BEM results are in excellent agreement with the FDM and FEM results.

Nowadays, knowledge and understanding of the propagation of acoustic waves of three-temperature nonlinear generalized magneto-thermoelasticity theory can be utilized by computer scientists and engineers, geotechnical and geothermal engineers, material science researchers and designers, and mechanical engineers for designing heat exchangers, semiconductor nanomaterials, and boiler tubes, as well as for chemists to observe the chemical reaction processes such as bond forming and bond breaking. In the application of three-temperature theories in advanced manufacturing technologies, with the development of soft machines and robotics in biomedical engineering and advanced manufacturing, acoustic displacement waves will be encountered more often where three-temperature nonlinear generalized magneto-thermoelasticity theory will turn out to be the best choice for thermomechanical analysis in the design and analysis of advanced ISMFGA structures using laser ultrasonics.

IntechOpen

IntechOpen

Author details

Mohamed Abdelsabour Fahmy
Faculty of Computers and Informatics, Suez Canal University, Ismailia, Egypt

*Address all correspondence to: mohamed_fahmy@ci.suez.edu.eg

IntechOpen

© 2020 The Author(s). Licensee IntechOpen. This chapter is distributed under the terms of the Creative Commons Attribution License (http://creativecommons.org/licenses/by/3.0), which permits unrestricted use, distribution, and reproduction in any medium, provided the original work is properly cited.

References

[1] Telschow KL, Conant RJ. Optical and thermal parameter effects on laser generated ultrasound. The Journal of the Acoustical Society of America. 1990;**88**: 1494-1502

[2] Hurley DH, Spicer JB, Wagner JW, Murray TW. Investigation of the anisotropic nature of laser-generated ultrasound in zinc and unidirectional carbon epoxy composites. Ultrasonics. 1998;**36**:355-360

[3] Bernstein JR, Spicer JB. Line source representation for laser-generated ultrasound in aluminum. The Journal of the Acoustical Society of America. 2000;**107**:1352-1357

[4] White R. Generation of elastic waves by transient surface heating. Journal of Applied Physics. 1963;**34**: 3559-3567

[5] Scruby C, Dewhurst R, Hutchins D, Palmer S. Quantitative studies of thermally-generated elastic waves in laser irradiated metals. Journal of Applied Physics. 1980;**51**:6210-6216

[6] Rose LRF. Point-source representation for laser generated ultra-sound. The Journal of the Acoustical Society of America. 1984;**75**: 723-732

[7] Doyle P. On epicentral waveforms for laser-generated ultrasound. Journal of Physics D: Applied Physics. 1986;**19**: 1613-1623

[8] McDonald F. Practical quantitative theory of photoacoustic pulse generation. Applied Physics Letters. 1989;**54**:1504-1506

[9] Spicer J. Laser ultrasonics in finite structures: Comprehensive modeling with supporting experiment [PhD thesis]. The Johns Hopkins University; 1991

[10] Fahmy MA. A new boundary element strategy for modeling and simulation of three temperatures nonlinear generalized micropolar-magneto-thermoelastic wave propagation problems in FGA structures. Engineering Analysis with Boundary Elements. 2019;**108**:192-200

[11] Fahmy MA. A new computerized boundary element model for three-temperature nonlinear generalized thermoelastic stresses in anisotropic circular cylindrical plate structures. In: Awrejcewicz J, Grzelczyk D, editors. Dynamical Systems Theory. London, UK: IntechOpen; 2019. pp. 1-17

[12] Fahmy MA. Boundary element model for nonlinear fractional-order heat transfer in magneto-thermoelastic FGA structures involving three temperatures. In: Ebrahimi F, editor. Mechanics of Functionally Graded Materials and Structures. London, UK: IntechOpen; 2019. pp. 1-22

[13] Fahmy MA. Boundary element mathematical modelling and boundary element numerical techniques for optimization of micropolar thermoviscoelastic problems in solid deformable bodies. In: Sivasankaran S, Nayak PK, Günay E, editors. Mechanics of Solid Deformable Bodies. London, UK: IntechOpen; 2020. pp. 1-21

[14] Fahmy MA. Boundary element modeling and optimization based on fractional-order derivative for nonlinear generalized photo-thermoelastic stress wave propagation in three-temperature anisotropic semiconductor structures. In: Sadollah A, Sinha TS, editors. Recent Trends in Computational Intelligence. London, UK: IntechOpen; 2020. pp. 1-16

[15] Abd-Alla AM, El-Naggar AM, Fahmy MA. Magneto-thermoelastic

problem in non-homogeneous isotropic cylinder. Heat and Mass Transfer. 2003; **39**:625-629

[16] Hu Q, Zhao L. Domain decomposition preconditioners for the system generated by discontinuous Galerkin discretization of 2D-3T heat conduction equations. Communications in Computational Physics. 2017;**22**: 1069-1100

[17] Sharma N, Mahapatra TR, Panda SK. Thermoacoustic behavior of laminated composite curved panels using higher-order finite-boundary element model. International Journal of Applied Mechanics. 2018;**10**:1850017

[18] Fahmy MA. A time-stepping DRBEM for magneto-thermo-viscoelastic interactions in a rotating nonhomogeneous anisotropic solid. International Journal of Applied Mechanics. 2011;**3**:1-24

[19] Fahmy MA. A time-stepping DRBEM for the transient magneto-thermo-visco-elastic stresses in a rotating non-homogeneous anisotropic solid. Engineering Analysis with Boundary Elements. 2012;**36**: 335-345

[20] Fahmy MA. Numerical modeling of transient magneto-thermo-viscoelastic waves in a rotating nonhomogeneous anisotropic solid under initial stress. International Journal of Modeling. Simulation and Scientific Computing. 2012;**3**:1250002

[21] Fahmy MA. Transient magneto-thermo-viscoelastic stresses in a rotating nonhomogeneous anisotropic solid with and without a moving heat source. Journal of Engineering Physics and Thermophysics. 2012;**85**:950-958

[22] Fahmy MA. Transient magneto-thermo-elastic stresses in an anisotropic viscoelastic solid with and without moving heat source. Numerical Heat Transfer, Part A: Applications. 2012;**61**: 547-564

[23] Fahmy MA. Transient magneto-thermoviscoelastic plane waves in a non-homogeneous anisotropic thick strip subjected to a moving heat source. Applied Mathematical Modelling. 2012; **36**:4565-4578

[24] Fahmy MA. The effect of rotation and inhomogeneity on the transient magneto-thermoviscoelastic stresses in an anisotropic solid. ASME Journal of Applied Mechanics. 2012;**79**:1015

[25] Fahmy MA. Computerized Boundary Element Solutions for Thermoelastic Problems: Applications to Functionally Graded Anisotropic Structures. Saarbrücken: Lambert Academic Publishing (LAP); 2017

[26] Fahmy MA. Boundary Element Computation of Shape Sensitivity and Optimization: Applications to Functionally Graded Anisotropic Structures. Saarbrücken: Lambert Academic Publishing (LAP); 2017

[27] Fahmy MA. A time-stepping DRBEM for 3D anisotropic functionally graded piezoelectric structures under the influence of gravitational waves. In: Facing the Challenges in Structural Engineering, Sustainable Civil Infrastructures. Proceedings of the 1st GeoMEast International Congress and Exhibition (GeoMEast 2017); 15–19 July 2017; Sharm El Sheikh, Egypt. 2017. pp. 350-365

[28] Fahmy MA. 3D DRBEM modeling for rotating initially stressed anisotropic functionally graded piezoelectric plates. In: Proceedings of the 7th European Congress on Computational Methods in Applied Sciences and Engineering (ECCOMAS 2016); 5–10 June 2016; Crete Island, Greece. pp. 7640-7658

[29] Fahmy MA. Boundary element solution of 2D coupled problem in

anisotropic piezoelectric FGM plates. In: Proceedings of the 6th International Conference on Computational Methods for Coupled Problems in Science and Engineering (Coupled Problems 2015); 18–20 May 2015; Venice, Italy. pp. 382-391

[30] Fahmy MA. The DRBEM solution of the generalized magneto-thermo-viscoelastic problems in 3D anisotropic functionally graded solids. In: Proceedings of the 5th International Conference on Coupled Problems in Science and Engineering (Coupled Problems 2013); 17–19 June 2013; Ibiza, Spain. pp. 862-872

[31] Fahmy MA. A computerized boundary element model for simulation and optimization of fractional-order three temperatures nonlinear generalized piezothermoelastic problems based on genetic algorithm. In: AIP Conference Proceedings 2138 of Innovation and Analytics Conference and Exihibiton (IACE 2019); 25-28 March 2019; Sintok, Malaysia. p. 030015

[32] Soliman AH, Fahmy MA. Range of applying the boundary condition at fluid/porous Interface and evaluation of beavers and Joseph's slip coefficient using finite element method. Computation. 2020;**8**:14

[33] Eskandari AH, Baghani M, Sohrabpour S. A time-dependent finite element formulation for thick shape memory polymer beams considering shear effects. International Journal of Applied Mechanics. 2019;**10**:1850043

[34] Huang R, Zheng SJ, Liu ZS, Ng TY. Recent advances of the constitutive models of smart materials—Hydrogels and shape memory polymers. International Journal of Applied Mechanics. 2020;**12**:2050014

[35] Othman MIA, Khan A, Jahangir R, Jahangir A. Analysis on plane waves through magneto-thermoelastic microstretch rotating medium with temperature dependent elastic properties. Applied Mathematical Modelling. 2019;**65**:535-548

[36] Ezzat MA, El-Bary AA. Application of fractional order theory of magneto-thermoelasticity to an infinite perfect conducting body with a cylindrical cavity. Microsystem Technologies. 2017; **23**:2447-2458

[37] Fahmy MA. A new computerized boundary element algorithm for cancer modeling of cardiac anisotropy on the ECG simulation. Asian Journal of Research in Computer Science. 2018;**2**: 1-10

[38] Fahmy MA. Implicit-explicit time integration DRBEM for generalized magneto-thermoelasticity problems of rotating anisotropic viscoelastic functionally graded solids. Engineering Analysis with Boundary Elements. 2013; **37**:107-115

[39] Fahmy MA. Generalized magneto-thermo-viscoelastic problems of rotating functionally graded anisotropic plates by the dual reciprocity boundary element method. Journal of Thermal Stresses. 2013;**36**:1-20

[40] Fahmy MA. A three-dimensional generalized magneto-thermo-viscoelastic problem of a rotating functionally graded anisotropic solids with and without energy dissipation. Numerical Heat Transfer, Part A: Applications. 2013;**63**:713-733

[41] Fahmy MA. A 2-D DRBEM for generalized magneto-thermo-viscoelastic transient response of rotating functionally graded anisotropic thick strip. International Journal of Engineering and Technology Innovation. 2013;**3**:70-85

[42] Fahmy MA, Salem AM, Metwally MS, Rashid MM. Computer implementation of the DRBEM for

studying the generalized thermoelastic responses of functionally graded anisotropic rotating plates with one relaxation time. International Journal of Applied Science and Technology. 2013; **3**:130-140

[43] Fahmy MA, Salem AM, Metwally MS, Rashid MM. Computer implementation of the DRBEM for studying the classical uncoupled theory of thermoelasticity of functionally graded anisotropic rotating plates. International Journal of Engineering Research and Applications. 2013;**3**: 1146-1154

[44] Fahmy MA. A computerized DRBEM model for generalized magneto-thermo-visco-elastic stress waves in functionally graded anisotropic thin film/substrate structures. Latin American Journal of Solids and Structures. 2014;**11**:386-409

[45] Fahmy MA, Salem AM, Metwally MS, Rashid MM. Computer implementation of the DRBEM for studying the classical coupled thermoelastic responses of functionally graded anisotropic plates. Physical Science International Journal. 2014;**4**: 674-685

[46] Fahmy MA, Salem AM, Metwally MS, Rashid MM. Computer implementation of the DRBEM for studying the generalized thermo elastic responses of functionally graded anisotropic rotating plates with two relaxation times. British Journal of Mathematics & Computer Science. 2014;**4**:1010-1026

[47] Fahmy MA. A 2D time domain DRBEM computer model for magneto-thermoelastic coupled wave propagation problems. International Journal of Engineering and Technology Innovation. 2014;**4**:138-151

[48] Brebbia CA, Telles JCF, Wrobel L. Boundary Element Techniques in Engineering. New York: Springer-Verlag; 1984

[49] Wrobel LC, Brebbia CA. The dual reciprocity boundary element formulation for nonlinear diffusion problems. Computer Methods in Applied Mechanics and Engineering. 1987;**65**:147-164

[50] Partridge PW, Wrobel LC. The dual reciprocity boundary element method for spontaneous ignition. International Journal for Numerical Methods in Engineering. 1990;**30**:953-963

[51] Partridge PW, Brebbia CA. Computer implementation of the BEM dual reciprocity method for the solution of general field equations. Communications in Applied Numerical Methods. 1990;**6**:83-92

[52] Partridge PW, Brebbia CA, Wrobel LC. The Dual Reciprocity Boundary Element Method. Southampton: Computational Mechanics Publications; 1992

[53] Gaul L, Kögl M, Wagner M. Boundary Element Methods for Engineers and Scientists. Berlin: Springer-Verlag; 2003

[54] Fahmy MA, Al-Harbi SM, Al-Harbi BH. Implicit time-stepping DRBEM for design sensitivity analysis of magneto-thermo-elastic FGA structure under initial stress. American Journal of Mathematical and Computational Sciences. 2017;**2**:55-62

[55] Fahmy MA. The effect of anisotropy on the structure optimization using golden-section search algorithm based on BEM. Journal of Advances in Mathematics and Computer Science. 2017;**25**:1-18

[56] Fahmy MA. DRBEM sensitivity analysis and shape optimization of rotating magneto-thermo-viscoelastic FGA structures using golden-section

search algorithm based on uniform bicubic B-splines. Journal of Advances in Mathematics and Computer Science. 2017;**25**:1-20

[57] Fahmy MA. A predictor-corrector time-stepping DRBEM for shape design sensitivity and optimization of multilayer FGA structures. Transylvanian Review. 2017;**XXV**: 5369-5382

[58] Fahmy MA. Shape design sensitivity and optimization for two-temperature generalized magneto-thermoelastic problems using time-domain DRBEM. Journal of Thermal Stresses. 2018;**41**: 119-138

[59] Fahmy MA. Boundary element algorithm for modeling and simulation of dual-phase lag bioheat transfer and biomechanics of anisotropic soft tissues. International Journal of Applied Mechanics. 2018;**10**:1850108

[60] Fahmy MA. Shape design sensitivity and optimization of anisotropic functionally graded smart structures using bicubic B-splines DRBEM. Engineering Analysis with Boundary Elements. 2018;**87**:27-35

[61] Fahmy MA. Modeling and optimization of anisotropic viscoelastic porous structures using CQBEM and moving asymptotes algorithm. Arabian Journal for Science and Engineering. 2019;**44**:1671-1684

[62] Fahmy MA. Boundary element modeling and simulation of biothermomechanical behavior in anisotropic laser-induced tissue hyperthermia. Engineering Analysis with Boundary Elements. 2019;**101**: 156-164

[63] Fahmy MA, Al-Harbi SM, Al-Harbi BH, Sibih AM. A computerized boundary element algorithm for modeling and optimization of complex magneto-thermoelastic problems in MFGA structures. Journal of Engineering Research and Reports. 2019;**3**:1-13

[64] Fahmy MA. A new LRBFCM-GBEM modeling algorithm for general solution of time fractional order dual phase lag bioheat transfer problems in functionally graded tissues. Numerical Heat Transfer, Part A: Applications. 2019;**75**:616-626

[65] Fahmy MA. Design optimization for a simulation of rotating anisotropic viscoelastic porous structures using time-domain OQBEM. Mathematics and Computers in Simulation. 2019;**66**: 193-205

[66] Fahmy MA. A new convolution variational boundary element technique for design sensitivity analysis and topology optimization of anisotropic thermo-poroelastic structures. Arab Journal of Basic and Applied Sciences. 2020;**27**:1-12

[67] Zenkour A, Allehaibi AM, Fahmy MA. Three-temperature nonlinear generalized magneto-thermoelastic stresses in anisotropic cylindrical shells. Journal of Applied and Computational Mechanics. DOI: 10.22055/jacm.2020.33101.2151

[68] Pazera E, Jędrysiak J. Effect of microstructure in thermoelasticity problems of functionally graded laminates. Composite Structures. 2018; **202**:296-303

[69] Xiong QL, Tian XG. Generalized magneto-thermo-microstretch response during thermal shock. Latin American Journal of Solids and Structures. 2015; **12**:2562-2580